Phase behavior of liquid crystals confined by smooth walls

Haiko Steuer* and Siegfried Hess
Institut für Theoretische Physik, Technische Universität Berlin, PN7-1, Hardenbergstrasse 36, D-10623 Berlin, Germany

Martin Schoen
Stranski-Laboratorium für Physikalische und Theoretische Chemie, Technische Universität Berlin, TC7, Straße des 17, Juni 124, D-10623 Berlin, Germany

(Received 12 November 2003; published 31 March 2004)

Monte Carlo simulations for a simple model liquid crystal are presented. The influence of flat walls on the phase behavior is analyzed for two different anchoring mechanisms, one favoring homeotropic alignment and one simulating a twisted nematic cell without external fields, e.g., two walls with different homogeneous planar alignment. The simulations are performed in the constant pressure ensemble. The box volume may change in the directions perpendicular to the wall normal. The isotropic-nematic phase transition in the bulk system is first studied for different isobars. For the weak first order transition we do not observe any hysteresis down to a temperature accuracy of $\Delta T = 0.001$. The isotherm $T = 1$ is then studied in the bulk as well as in the confined geometries. The walls stabilize the positional order in the systems due to the formation of layers. The orientational order is weakly stabilized.

DOI: 10.1103/PhysRevE.69.031708 PACS number(s): 61.30.Cz, 61.30.Hn, 64.60.Cn, 64.70.Md

I. INTRODUCTION

Liquid crystals are very useful for many applications due to their dual nature and easy response to surface forces [1]. In 2002, liquid crystal displays became the most produced display type world wide. Therefore, the physics of confined liquid crystals is an important subject from the technological point of view. Furthermore, the influence of confinement on the phase behavior of liquid crystals is of high academic interest. The interplay between bulk and surface forces gives rise to a complex phase behavior. In experiments the confinement is found to induce capillary condensation [2].

Until now, there have been many theoretical studies of liquid crystals in restricted geometries with help of both molecular simulations [3–15] and density functional theories [16–22] or combinations of both [23–25]. Often used interaction potentials are the Gay-Berne [26,27] potential [4–6,8,11], hard particles with cylindrical symmetry [10,16,23,25] or a kind of Lebwohl-Lasher [28] model [3,9,12,13,15].

For a recently presented simple interaction potential, the bulk phase behavior was determined analytically [29]. In Monte Carlo simulations [30] these results were confirmed. A nematic phase was observed and the isotropic-nematic phase transition was studied in greater detail for some densities. Here, further Monte Carlo studies of this model are carried out. Simulations with confining flat walls reveal the influence of different kinds of substrates on the phase behavior and alignment effects of this model liquid crystal. We use two different kinds of substrates. The first one is modeled without an orientation dependent wall-particle interaction which results in homeotropic alignment. The second is modeled such that both walls prefer homogeneous planar alignment, but with 90 degrees difference between the azimuthal angles at the walls. The nematic phase is then characterized by an inhomogeneous director field, the physics is that of a twisted nematic cell without any orienting field.

This paper proceeds as follows. In Sec. II we briefly review the interaction potential for the model liquid crystal fluid and give insight in the fluid-wall interaction, which models a smooth wall. Some details of the Monte Carlo simulations, which were carried out each with constant pressure and constant temperature, as well as remarks about the observables, for which average values are obtained are given in Sec. III. In Sec. IV results of the computer simulations are presented and discussed. The isotropic-nematic phase transitions are studied for two different fluid-wall interactions, leading to different alignments, and are compared with the bulk transition.

II. MODEL SYSTEM

We consider a fluid composed of (effectively) axisymmetric particles whose orientation is characterized by a unit vector $\hat{\mathbf{u}}$ parallel to the figure axis. The interaction potential between two particles located at the positions $\mathbf{r}_1$ and $\mathbf{r}_2$ with orientations $\hat{\mathbf{u}}_1$ and $\hat{\mathbf{u}}_2$ depends on the three vectors $\mathbf{r}=\mathbf{r}_2-\mathbf{r}_1$, $\hat{\mathbf{u}}_1$, and $\hat{\mathbf{u}}_2$. The interaction energy for two fluid particles is written as [29]

$$\Phi_{ff}(\mathbf{r},\hat{\mathbf{u}}_1,\hat{\mathbf{u}}_2)=4\{r^{-12}-r^{-6}[1+\Psi(\hat{\mathbf{r}},\hat{\mathbf{u}}_1,\hat{\mathbf{u}}_2)]\}, \quad (1)$$

where $\mathbf{r}=r\hat{\mathbf{r}}$. Standard Lennard-Jones (LJ) units are used, i.e., the length r and the energy Φ are expressed in LJ ''diameter,'' and potential depth, respectively [31]. The anisotropy in the attractive term is described by

$$\Psi(\hat{\mathbf{r}},\hat{\mathbf{u}}_1,\hat{\mathbf{u}}_2)=5\varepsilon_1 \mathrm{P}_2(\hat{\mathbf{u}}_1\cdot\hat{\mathbf{u}}_2)+5\varepsilon_2[\mathrm{P}_2(\hat{\mathbf{u}}_1\cdot\hat{\mathbf{r}})+\mathrm{P}_2(\hat{\mathbf{u}}_2\cdot\hat{\mathbf{r}})]. \quad (2)$$

Here $\mathrm{P}_2(x)=(3x^2-1)/2$ is the second Legendre polynomial. Note that $\hat{\mathbf{u}}_j$ is equivalent to $-\hat{\mathbf{u}}_j$, so the head-tail symmetry

*Electronic address: haiko@physik.tu-berlin.de

is satisfied. In the calculations the potential was cut off at a distance $r_c=3$. The anisotropy coefficients ε_i are chosen to be $\varepsilon_1=0.04$ and $\varepsilon_2=-0.08$. In this case the side-side configuration is energetically favored, since the side-side interaction potential $\Phi_{ff}^{\text{side-side}}(r):=\Phi_{ff}(\mathbf{e}_x r,\mathbf{e}_z,\mathbf{e}_z)$ has a much deeper minimum than, for example, the end-end potential $\Phi_{ff}^{\text{end-end}}(r):=\Phi_{ff}(\mathbf{e}_z r,\mathbf{e}_z,\mathbf{e}_z)$.

We consider our system both in a bulk state and with walls forming a confined geometry. The boundary conditions for our system without walls are periodic in all three directions. This means, that a particle at the margin of the simulation box can interact with a particle at the opposite side.

In simulations with walls we have to change the boundary condition in one direction. If the simulation box has the edges d_x, d_y, and d_z, we place two flat walls at the planes $z=z_{1/2}=\pm d_z/2$ parallel to the xy plane. Therefore we do not apply periodic boundary conditions in the z direction. The walls consist of particles interacting with fluid particles with orientation $\hat{\mathbf{u}}$ at distant r according to a Lennard-Jones type potential $\phi_{fw}(r,\hat{\mathbf{u}})=4[r^{-12}-r^{-6}g_w(\hat{\mathbf{u}})]$ with the anchoring function $g_w(\hat{\mathbf{u}})$. It is chosen to model the desired alignment. For $g_w(\hat{\mathbf{u}})=(\hat{\mathbf{u}}\cdot\hat{\mathbf{a}}_w)^2$ we get homogeneous planar alignment at the wall with orientations parallel to the unit vector $\hat{\mathbf{a}}_w$, for $g_w(\hat{\mathbf{u}})=1$ we get homeotropic alignment. A twisted nematic cell can be modeled using the anchoring functions $g_1(\hat{\mathbf{u}})=\hat{u}_x^2$ and $g_2(\hat{\mathbf{u}})=\hat{u}_y^2$. The fluid-wall potential is cut off at distance $r_c=3$.

Now we could put particles on a lattice in the solid wall (discrete walls) and let our particles interact pairwise with them [8]. Another possibility is much easier and handles the walls continously [4,32,33]. We follow the latter way and assume a smooth wall with a particle density of ρ_w. By integrating the wall-fluid potential over the wall w we get

$$\Phi_{fw}(\mathbf{r},\hat{\mathbf{u}})=\rho_w\int_w \phi_{fw}(\|\mathbf{r}-\mathbf{r}_w\|,\hat{\mathbf{u}})d^2r_w$$
$$=2\pi\rho_w\left(\frac{4}{10}(z-z_w)^{-10}-(z-z_w)^{-4}g_w(\hat{\mathbf{u}})\right), \tag{3}$$

where $\mathbf{r}=(x,y,z)$ is the position of the fluid particle.

III. DETAILS ON THE *NPT* MONTE CARLO METHOD FOR THE CONFINED FLUID

A system consisting of N uniaxial particles, where the fluid-fluid pair potential is given by Eq. (1) and the fluid-wall potential is given by Eq. (3), is considered.

The total potential energy for a configuration $\mathbf{\Gamma}^c\equiv(\mathbf{r}_1,\hat{\mathbf{u}}_1,\ldots\mathbf{r}_N,\hat{\mathbf{u}}_N)$ is given as

$$\Phi_{\text{tot}}=\sum_{j=1}^{N}\left[\sum_{i=j+1}^{N}\Phi_{ff}(\mathbf{r}_{ij},\hat{\mathbf{u}}_i,\hat{\mathbf{u}}_j)+\sum_{w=1}^{2}\Phi_{fw}(\mathbf{r}_j,\hat{\mathbf{u}}_j)\right], \tag{4}$$

where $\mathbf{r}_{ij}=\mathbf{r}_i-\mathbf{r}_j$. In the simulations up to $N=1000$ particles were studied at a given temperature T and a given lateral pressure $P_\parallel$. If $\mathbf{P}$ is the pressure tensor, then $P_\parallel=\frac{1}{2}(P_{xx}+P_{yy})$ takes into account forces parallel to the walls. In bulk simulations for isotropic phases, the scalar pressure $P=\frac{1}{3}(P_{xx}+P_{yy}+P_{zz})$ equals the lateral pressure $P_\parallel$. For an observable A which depends on the configuration only, i.e., $A=A(\mathbf{\Gamma}^c)$, we can obtain average values in the NPT ensemble through

$$\langle A\rangle\approx\frac{1}{M_2-M_1}\sum_{i=M_1+1}^{M_2}A(\mathbf{\Gamma}_i^c). \tag{5}$$

The set of configurations $\{\mathbf{\Gamma}_i^c\}_{i=1,\ldots,M_2}$ is produced as follows according to Metropolis' algorithm [34], which is adapted for the constant pressure ensemble [31,35]: At the beginning we randomly choose a starting configuration $\mathbf{\Gamma}_1^c$ in a box of volume $V_1=d_x d_y d_z$. The z length must be $d_z=z_{w=2}-z_{w=1}$. For a given particle we randomly change either the orientation or the position. Then we calculate the associated change in energy $\Delta\Phi_{\text{tot}}$ and accept the new configuration with probability $\min[1,\exp(-\Delta\Phi_{\text{tot}}/k_{\text{B}}T)]$. The range of the changes in positions is adjusted during the simulations in order to gain fast convergence to equilibrium. The rotation angle range for the change of the orientations is set to $\pi/10$. The particles are organized in boxes and neighbor lists to save time for calculating particle distances. Neighbor lists must be updated in certain intervals on account of particle diffusion. After all particles have been taken into account we try to change the volume. Thereby we keep the distance d_z between the walls constant and only change d_x and d_y with the same random factor $c\in(0.995,1.005)$, i.e., $d_x^{\text{new}}=cd_x$ and $d_y^{\text{new}}=cd_y$. The positions of the fluid particles are scaled accordingly: $x^{\text{new}}=cx$ and $y^{\text{new}}=cy$. The acceptance probability of this volume change $\Delta V=V_{\text{new}}-V_{\text{old}}$ is given through

$$\min\left\{1,\left(\frac{V_{\text{new}}}{V_{\text{old}}}\right)^N\exp\left(-\frac{\Delta\Phi_{\text{tot}}+P_\parallel\Delta V}{k_{\text{B}}T}\right)\right\}. \tag{6}$$

The factor $(V_{\text{new}}/V_{\text{old}})^N=c^{2N}$ comes from substitutions $s_{j\nu}:=r_{j\nu}/d_\nu$ and $d^3r_j=Vd^3s_j$ in the partition function which has to be done in order to handle the scaling of the positions [36,37]. Without this substitution the positions would implicitly depend on the other integration variable, namely, the volume. The change of potential energy $\Delta\Phi_{\text{tot}}$ must be calculated with some caution. The cut off at distance r_c should not lead to the artificial effect that one pair of particles may be considered for one volume but not for the other (bigger) one. Therefore, we cut off each pair interaction according to a common criterion $0.5(r_{\text{old}}+r_{\text{new}})>r_c$. Finally we arrive at a new configuration $\mathbf{\Gamma}_2^c$ at volume V_2. After M_1 Monte Carlo steps of this kind we find that our observables fluctuate around some average value. Typical numbers in our simulations were $M_1=10\,000$ and $M_2=100000$ with higher numbers in the vicinity of phase transitions.

Quantities calculated are the internal energy E, the energy fluctuation ΔE as well as the nematic and smectic order parameters S_2 and ϱ_1, respectively. For the internal energy one has

$$E = 3Nk_BT + \langle \Phi_{tot} \rangle. \tag{7}$$

The fluctuation of the internal energy can be cast as

$$\Delta E = \sqrt{\langle \Phi_{tot}^2 \rangle - \langle \Phi_{tot} \rangle^2}, \tag{8}$$

because N and T are fixed in our simulations.

A. Nematic order parameter

Nematic order is characterized by the so-called Maier-Saupe order parameter S_2^{MS} [38–40] which is the largest eigenvalue of the alignment tensor [41] $\mathbf{S} := \frac{3}{2}\langle \mathbf{Q} \rangle$, where

$$\mathbf{Q} = \frac{1}{N} \sum_{j=1}^{N} \overline{\hat{\mathbf{u}}_j \hat{\mathbf{u}}_j}$$

for a homogeneous system. The symbol $\overline{a_{\nu\mu}} = \frac{1}{2}(a_{\nu\mu} + a_{\mu\nu}) - \frac{1}{3} a_{\lambda\lambda} \delta_{\nu\mu}$ denotes the symmetric traceless part of a tensor $a_{\nu\mu}$. For isotropic phases S_2^{MS} vanish. In our Monte Carlo simulations an isotropic phase is typically characterized by a nematic order parameter below 0.1. The nematic order parameter does not completely vanish due to the finite size of the simulation system. Perfect alignment $\hat{\mathbf{u}}_j = \mathbf{n}$ corresponds to $S_2^{MS} = 1$. For the nematic phase we expect typical values of $S_2^{MS} \gtrsim 0.4$. For uniaxial phases S_2 is equal to the quantity

$$S_2 = \left\langle \sqrt{\frac{3}{2}} \|\mathbf{Q}\| \right\rangle, \tag{10}$$

which we use as nematic order parameter.

B. Smectic order parameter

A smectic order parameter should be sensitive to the formation of layers. Of course, layers may also occur in solid phases. Any periodicity of the particle density $\varrho(\mathbf{r})$ should lead to a high smectic order parameter. Usually, the smectic order parameter ϱ_1 is the first coefficient of the Fourier sum of the particle density

$$\varrho(\mathbf{r}) = \varrho_0 + \sum_{k=1}^{\infty} \varrho_k \cos\left(\frac{2\pi k \mathbf{n} \cdot \mathbf{r}}{d} - \phi \right). \tag{11}$$

The periodicity d, the layer normal $\mathbf{n}$ and the offset ϕ are unknown. For $\phi = 0$ one layer should lie in the origin of the coordinate system. For a smectic-A phase the layer normal should be equal to the director and can therefore be extracted from the alignment tensor. But the dependency of ϱ_1 on $\mathbf{n}$ is very critical so that these results are not very satisfactory.

In the case of walls parallel to the xy plane, however, we already know the expected layer normal $\mathbf{n} = \mathbf{e}_z$. Next we can get rid of the offset ϕ by calculating the Fourier coefficient of the complex exponential function rather than that of the cosine. Finally we have

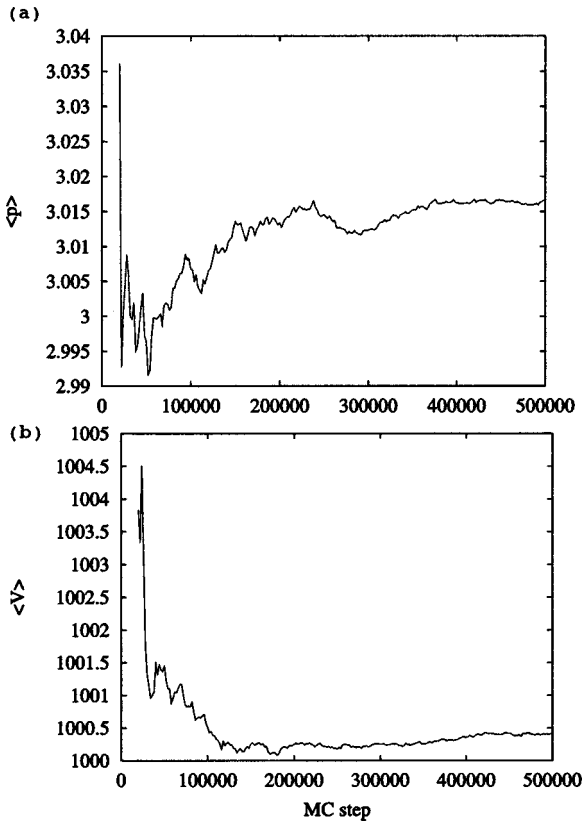

FIG. 1. $N = 800$ particle at temperature $T = 1.4$. (a) Average pressure for a NVT run at $V = 1000$. (b) Average volume for a NPT run at $P = 3.0168$.

$$\varrho_1 = \left\langle \left| \frac{1}{N} \sum_{j=1}^{N} \exp\left(\frac{2\pi i z_j}{d} \right) \right| \right\rangle. \tag{12}$$

This was also used [42] as a positional order parameter, motivated through the static structure factor. The remaining problem of achieving the periodicity d can be solved by just calculating $\varrho_1(d)$ in the expected range of d and then taking the maximum [43]. Here the range for the expected periodicity is chosen to be $d \in [0.7, 1.3]$.

C. Test of algorithm

To test our NPT algorithm in the bulk we first simulate $N = 800$ particles at temperature $T = 1.4$ in a cubic box of fixed volume $V = 10^3$ (NVT ensemble). The result is shown in Fig. 1(a). The average pressure tensor is calculated with help of

$$P^{\nu\mu} = \frac{Nk_BT}{V} \delta^{\nu\mu} + \frac{1}{V} \left\langle \sum_i \sum_{j<i} (r_i^\nu - r_j^\nu) F_{ij}^\mu \right\rangle, \tag{13}$$

where $\mathbf{F}_{ij} = -\partial / \partial \mathbf{r}_j \Phi_{ff}(\mathbf{r}_j - \mathbf{r}_i, \hat{\mathbf{u}}_i, \hat{\mathbf{u}}_j)$ is the force acting on particle j due to particle i. In the NVT simulation the scalar pressure P is found to be $P \approx 3.02$. Now we run a simulation with variable volume and fixed pressure $P_\parallel = 3.02$. This results in a average volume of $V \approx 1000.4$. The constant pressure simulations with a desired lateral pressure $P_\parallel$ are ex-

pected to fulfill $P_{xx}=P_{yy}=P_{\parallel}$. The component P_{zz} may differ in the inhomogeneous system with walls. For all our NPT calculations we found this expectation to be fulfilled in the limit of accuracy, which can be estimated from fluctuations of P_{xx} and P_{yy}.

D. Boundaries

Because of the wall influence the system is no longer homogeneous. Therefore we have to define some local observables. For example, we define the density $\rho(z)$ or the local order parameter $S_2(z)$ in the following way. The box is uniformly cut into layers parallel to the wall. Such a layer may typically have the width $\Delta z=0.2$ in Lennard-Jones units leading to a layer volume of $V_L=V(\Delta z/d_z)$. Then we count the particles for each layer $N(z)$, which leads after averaging to the density profile $\rho(z)=\langle N(z)/V_L\rangle$. The particles in each layer can be used to define a local alignment tensor $\mathbf{Q}(z)$. We average its norm to get

$$S_2(z)=\left\langle \sqrt{\frac{3}{2}}\|\mathbf{Q}(z)\| \right\rangle .$$

In order to compare the results for the bulk system with these numbers for the confined systems we should be able to measure the bulk density even in the simulation box with walls. We do this by taking into account for the density measurement only particles near the middle of the simulation box, which is far from the walls. The relevant region is chosen to be half of the whole box volume.

IV. RESULTS

Monte Carlo results from the NPT simulations will be presented for the bulk and the confined system (with homeotropic anchoring and with twisted homogeneous planar anchoring). For all simulations the z length of the simulation box is set to $d_z=15$ and the number of particles to $N=1000$.

A. The bulk system

For the bulk system it would not be necessary to restrict the NPT volume changes to the x and y directions. However we want to have the bulk behavior only as a reference for the restricted geometries and therefore we perform the bulk simulations in the same manner as the simulations with walls, namely, let the volume breath only in the x and y directions.

The isotropic-nematic (IN) phase transition is first studied for different isobars with pressure values $P_{\parallel}=0.1$, $P_{\parallel}=0.3$, $P_{\parallel}=0.5$, $P_{\parallel}=0.7$, and $P_{\parallel}=1.0$. Each simulation was done with $N=1000$ particles in a box with length $d_z=15$ and variable d_x and d_y. In Fig. 2 we show the density and nematic order parameter as functions of temperature, which was lowered until one enters the regime of nematic phases. During a cooling series we start a new run (with a slightly lowered temperature) with an initial configuration and volume taken from the end of the former simulation. The transition temperature T_{IN} is found to be between 0.88 and 0.96 depending on the pressure, at which the cooling procedure was performed. We also simulated the heating procedures back into the isotropic phase and were not able to observe any hysteresis in the accuracy of temperature steps we chose, even if we lowered ΔT to 0.001. This can be understood because of the weakness of the first order phase transition, which is typical for the IN transition [44]. The main result of these simulations is that for lower pressure values we get a lower T_{IN}.

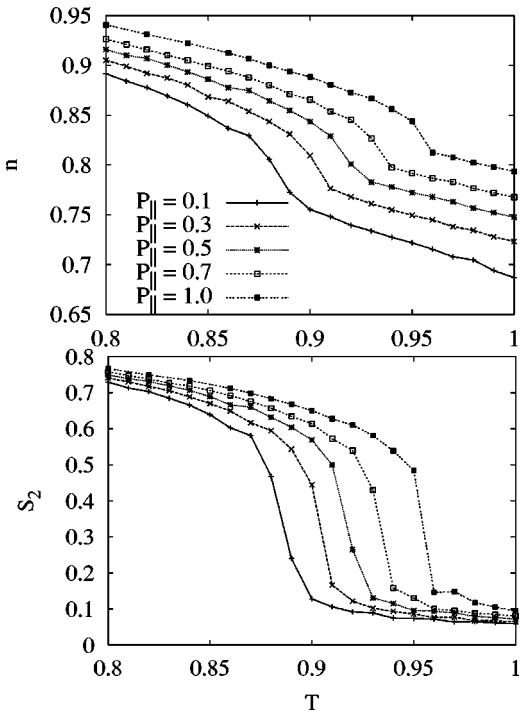

FIG. 2. Isotropic-nematic phase transition through cooling for different isobars. The number density n and the nematic order parameter S_2 are plotted vs the temperature T for different pressure values $P_{\parallel}$.

We gain deeper insight into the phase behavior by studying, in addition, an isotherm. By choosing $T=1$ we will have to compress our system quite strongly to force a transition to an anisotropic phase. For this temperature we will present similar isotherms in a restricted geometry and compare them with the bulk results in order to gain insight into the influence of confinement on the phase behavior. Some results for the isotherm $T=1$ are shown in Fig. 3. We start with an isotropic fluid at low pressure $P_{\parallel}=0.1$. NPT runs for which $P_{\parallel}=0$ are notoriously difficult on account of a dramatic increase of volume fluctuations as P goes to zero. The nematic order parameter S_2 as well as the smectic order parameter ϱ_1 are small in the isotropic phase, that is, lower than 0.1 for the finite-size system we observe. The average values for small pressures $P_{\parallel}<1$ confirm the results from the isobaric calculations for $T=1$ (Fig. 2). The isotropic-nematic phase transition takes place at $P_{IN}=1.7$, indicated through a peak in the energy fluctuation ΔE, which is proportional to the heat capacity. The phase transition is accompanied by a hardly visible jump in the number density around $n=0.85$ and by a remarkable jump in the nematic order parameter $S_2>0.4$. At

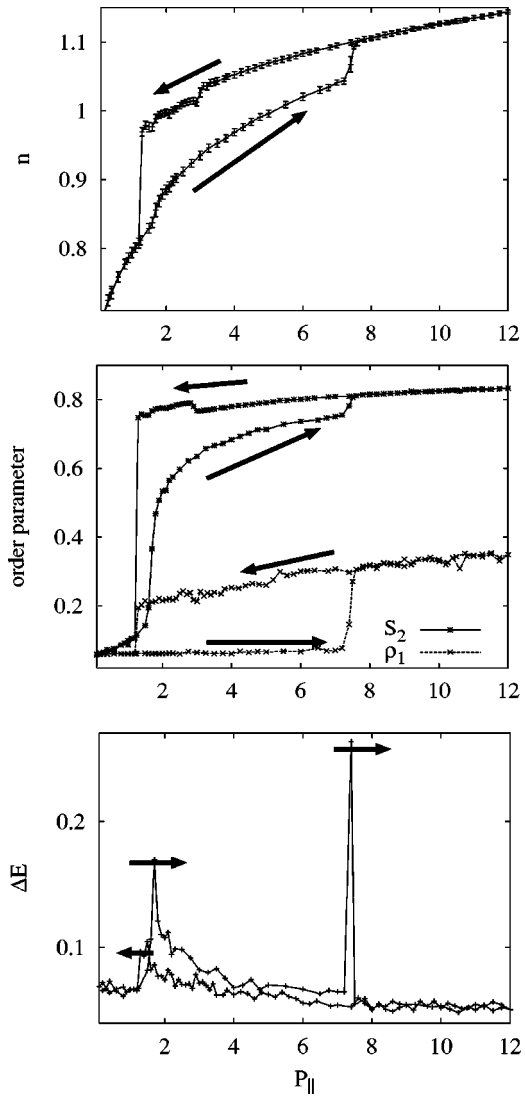

FIG. 3. Isotherm $T=1$ for the bulk system. For compression and expansion processes (indicated by the arrows) the number density n, the order parameters S_2 and ϱ_1 and the energy fluctuation ΔE are plotted as functions of the desired pressure $P_\parallel$.

$P_{NS}=7.4$ the system enters the solid state. This phase transition manifests itself clearly in the peak in ΔE and a discontinuity in n. The order parameters jump to higher values too. The smectic order parameter $\varrho_1 \approx 0.3$ indicates an increase in positional order. Snapshots of a configuration in the nematic phase at $P_\parallel=6$, where $S_2=0.74$ and a configuration in the solid state at $P_\parallel=8$, are shown in Fig. 4. In the solid state configuration, there are no layers perpendicular to the z direction. Because ϱ_1 is calculated assuming formation of layers perpendicular to z, its value remains small compared to 1.0. At $P_\parallel=12$ compression terminates and pressure is subsequently released in small steps. The system remains in the solid state even for small pressures. At $P_\parallel=3$ we observe a small increase in order where the pressure increases. This can be explained as a reorganization of crystal structure, which may happen in finite size and finite ''time'' Monte Carlo runs. Indicative for this is also the density jump around

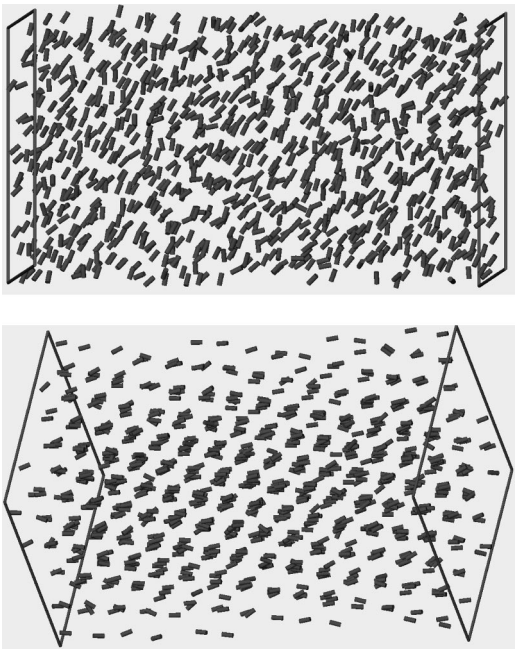

FIG. 4. Snapshots of bulk configurations at $P_\parallel=6$ (top), where the system is in a nematic phase and at $P_\parallel=8$ (bottom), where the system is in a solid state.

$P_\parallel=3$. We observe a strong hysteresis due to solidification, reflecting a pronounced first-order phase transition. The solid-nematic and nematic-isotropic transitions occur almost at the same pressure around $P_\parallel=1.4$.

B. The confined system with homeotropic alignment

To study the effect of confinement on the phase transitions observed, we now restrict the geometry by two flat walls (slab geometry). We begin by focusing on particle-wall interactions favoring homeotropic alignment. This can be modeled by setting the anchoring function $g(\hat{\mathbf{u}})=1$ thereby eliminating the orientation depending part in the interaction potential (3). Figure 5 shows the particle density, order parameters and energy fluctuation for the corresponding isotherm $T=1$. We again start with compressing the system in the isotropic phase. The smectic order parameter increases already for small pressures, but only slightly, indicating the formation of layers (see Fig. 6). The *IN* phase transition is smoother now and takes place at $P_{IN}=1.5$, that is, for a slightly lower pressure P_{IN} compared with the bulk system. For the slab geometry it is easier to form a nematic phase, because at least one layer is formed very early (see Fig. 7). In this layer the particle-particle interaction favors a side-side configuration (all $\hat{\mathbf{u}}_j$ parallel), resulting in homeotropic alignment. A high nematic order in the first layer near the wall is known for Gay-Berne particles too [6]. Therefore, the anchoring mechanism is responsible for the shifted *NI* transition. During this transition we observe a weak density jump and large peak in the energy fluctuation. Solidification takes place at $P_{NS}=2.5$, which is much lower than in the bulk. Layering turns out to be quite pronounced and causes positional order. The mere presence of a surface may, under fa-

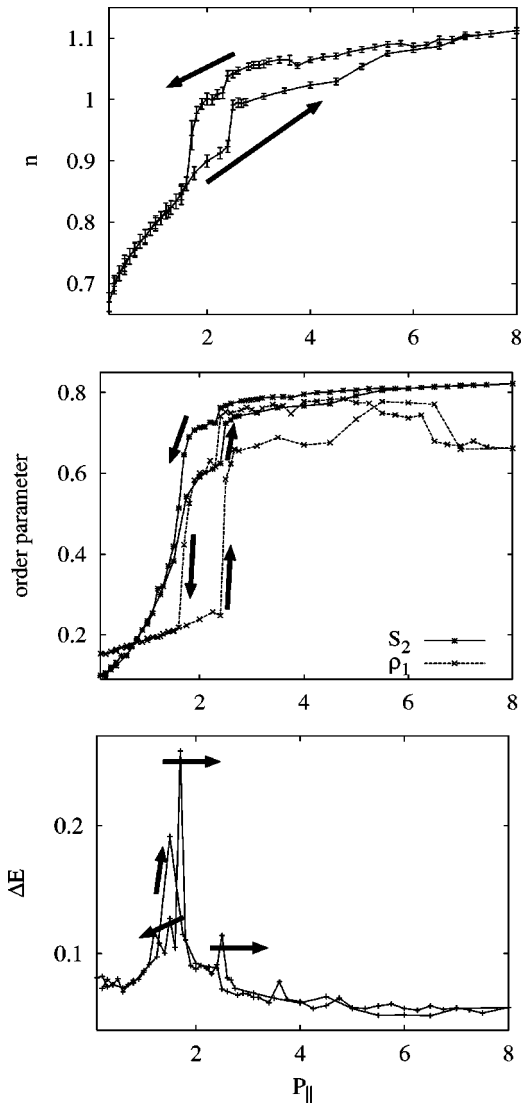

FIG. 5. Isotherm $T=1$ for the homeotropic aligned system. For compression and expansion processes (indicated by the arrows) the bulk number density n, the order parameters S_2 and ϱ_1 and the energy fluctuation ΔE are plotted as functions of the pressure $P_\parallel$.

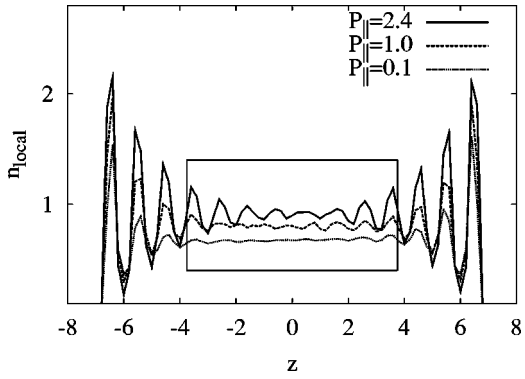

FIG. 6. Simulations with homeotropic alignment. Density profiles for $P_\parallel=0.1$, $P_\parallel=1.0$, and $P_\parallel=2.4$. The box indicates the region, where the bulk particle density is measured.

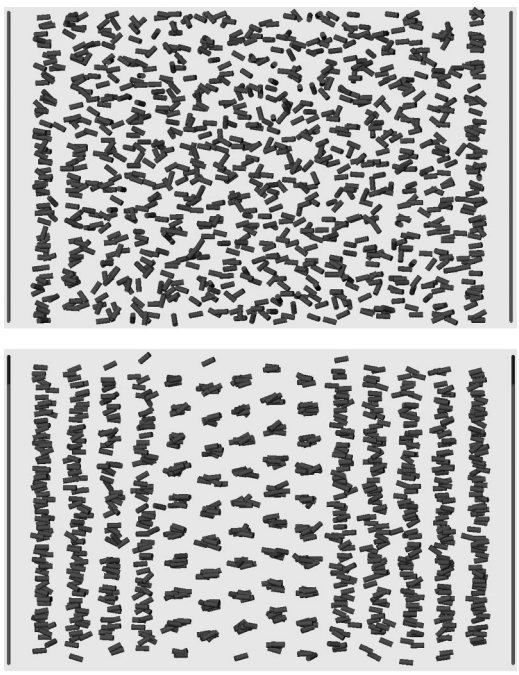

FIG. 7. Snapshots of configurations at $P_\parallel=1.5$ (top), where the system enters the nematic phase and at $P_\parallel=6$ (bottom), where the system is in a solid state.

vorable geometric conditions (i.e., suitable choice of d_z), support solidification if d_z is close to, such that, an unstrained solid can actually form. The nematic-solid phase transition is accompanied by a jump of the particle density and the order parameters. The crystal structure can be seen from two different perspectives in the snapshots. In Fig. 7 (bottom) the perspective is chosen such that the crystalline structure can be viewed in the middle of the cell. Rotations around the z axis would reveal the long-ranged positional order in the regions near the walls. So, the crystal is not perfect, but has some dislocations. To analyze the crystal structure in more detail, we focus on the second and third layer near the substrate ($z=-7.5$) for the final $P_\parallel=6$ con-

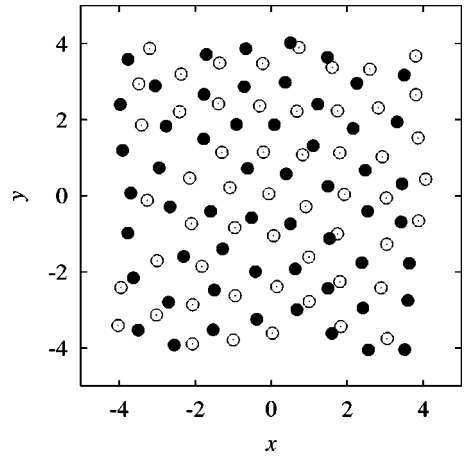

FIG. 8. Snapshot of layer configurations at $P_\parallel=6$. The empty circles are particles in the second layer, the filled circles are those of the third layer.

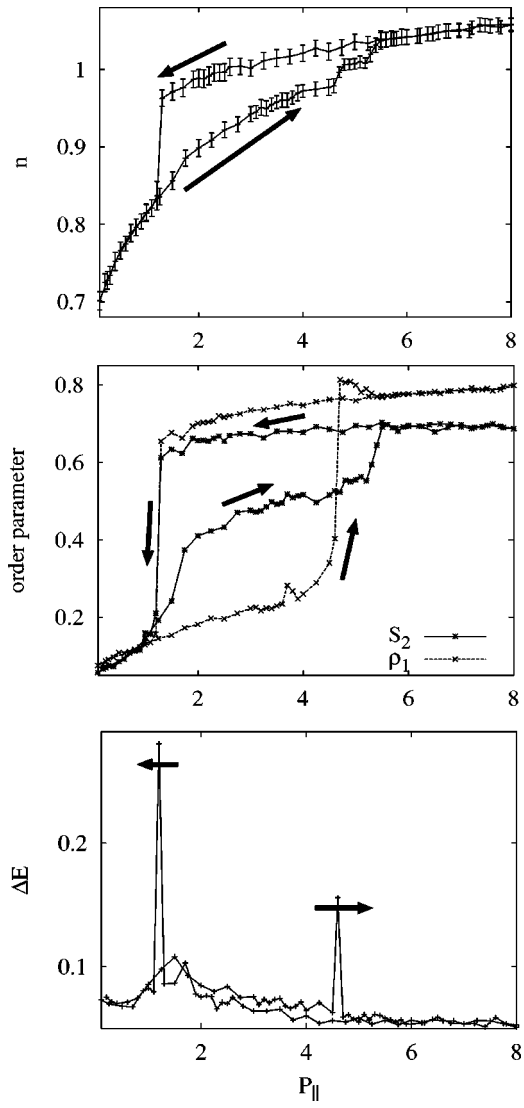

FIG. 9. Isotherm $T=1$ for the twisted homogeneous planar aligned system. For compression and expansion processes (indicated by the arrows) the bulk number density n, the order parameters S_2 and ϱ_1 and the energy fluctuation ΔE are plotted as functions of the pressure $P_\parallel$.

figuration (Fig. 8). The layers are found to consist of a two-dimensional hexagonal structure. For Gay-Berne particles it is already known that the first layer forms a two-dimensional lattice even in the bulk nematic phase. It is of importance for the onset of orientational order [6].

For pressures $P_\parallel > 5$ we find that the smectic order parameter is changing its value from time to time. This is indicative of a nonequilibrium situation, where the crystal structure reorganizes spontaneously. At $P_\parallel = 8$ we start expanding our system, observing again hysteresis. In the expansion process the nematic regime is quite narrow between $P_\parallel = 1.5$ and $P_\parallel = 1.2$, which is very similar to the bulk.

C. The confined system with twisted homogeneous planar alignment

Finally, we use the slab geometry again, but with different anchoring. The anchoring functions are now chosen to be

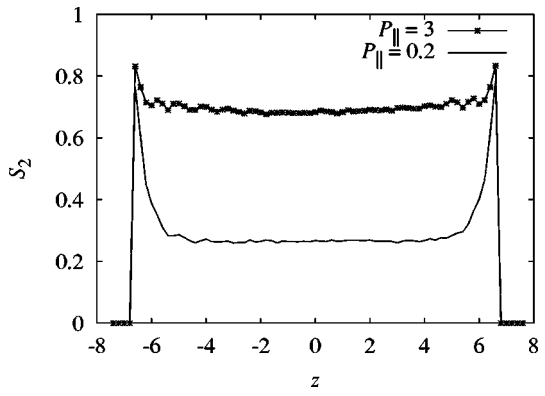

FIG. 10. Local nematic order parameter $S_2(z)$ for different pressures. At $P_\parallel = 3$ the system is in a nematic phase.

different for the two walls, namely, $g_1(\hat{\mathbf{u}}) = \hat{u}_x^2$ for the wall at $z = -7.5$ and $g_2(\hat{\mathbf{u}}) = \hat{u}_y^2$ for the wall at $z = 7.5$. This will favor homogeneous planar alignment at the walls with a director field, aligned along the x axis at $z = -7.5$ and along the y axis at $z = 7.5$. Therefore the director field is forced to be inhomogeneous. In the nematic phase, the simulation scenario will be equivalent to a twisted nematic cell without external fields. For such optical applications anchoring effects are very important [15,24]. In Fig. 9, again data for the isotherm $T = 1$ are given, where the system is compressed from $P_\parallel = 0.1$ to $P_\parallel = 8$ and then expanded back to $P_\parallel = 0.1$. During this procedure, isotropic, nematic, and solid phases are found as before. For low pressures $P_\parallel < P_{IN} = 1.5$ the system is in an isotropic phase. The order parameters increase with increasing pressure for the same reason as before. At $P_{IN} = 1.5$ the peak in the energy fluctuation indicates a transition in the nematic phase. Here, the nematic order parameter seems to remain quite small. The inhomogeneity of the director field keeps this global order parameter small. To find out the real value of the nematic order parameter, we consider local values of $S_2(z)$, as shown in Fig. 10. In the isotropic phase at $P_\parallel = 0.2$ the nematic order parameter turns out to be quite large (almost 0.3). This is due to the finite extent of layers into which the box was cut in order to measure local values. In average, each nonempty layer contains about 15 particles. In the nematic phase at $P_\parallel = 3$, where the global order parameter was lower than 0.5, we actually find local values of $S_2(z) \approx 0.7$. This number may be even larger for layers in the immediate vicinity of the walls. At $P_{NS} = 4.6$ solidification takes place, accompanied by a peak in the energy fluctuation and jumps of the particle density and the smectic order parameter. Solidification pressure is between those observed in the bulk and in the homeotropically aligned cell. It is more difficult to achieve long-ranged positional order if the orientational order is only short ranged due to the inhomogeneous director field. During some reorganization processes the crystal eventually reaches a configuration, where even the global nematic order parameter has values $S_2 > 0.6$. A snapshot of such a configuration (at $P_\parallel = 6$) together with one of the nematic phase is shown in Fig. 11. The surprisingly high global nematic order parameter $S_2 = 0.7$ can be rationalized as follows: In this crystal the right

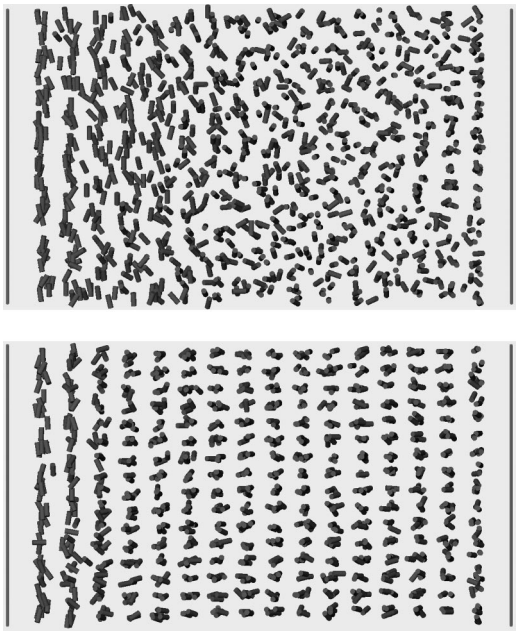

FIG. 11. Snapshots of configurations at $P_{\parallel}=3$ (top), where the system is in a nematic phase and at $P_{\parallel}=6$ (bottom), where the system is in a solid state.

wall has gained control over almost the whole cell. Therefore, apart from the first three layers near the left wall, the director is homogeneous. Because of a spontaneous break of symmetry caused by the right wall, its anchoring mechanism dominates the system. This can also be seen in Fig. 12, where the local azimuthal angle $\varphi(z)$ of the director $\mathbf{n}(z)$, defined through $\tan(\varphi)=n_x/n_y$, is plotted for different pressures. A value of $\varphi=90°$ belongs to the left wall at $z=-7.5$, where the particles are anchored along the x axis, and $\varphi=0°$ belongs to the anchoring at the right wall. In nematic phases (see $P_{\parallel}=2$ or $P_{\parallel}=4$) we find a linear tilt, so the director changes smoothly from one side to the other. Linear director profiles are known to occur for a lattice model liquid crystal confined in a hybrid cell [13]. For $P_{\parallel}=6$ the director jumps near the left wall and remains homogeneous otherwise. Expanding the simulation box in small pressure steps back to the isotropic phase we find again a large hysteresis. This time, we observe a single solid-isotropic transition at $P_{SI}=1.2$. During this transition the peak of the energy fluctuation as well as the jump in the particle density are very sharp. The nematic phase only occurs during the compression process, such that we have a monotropic nematic phase.

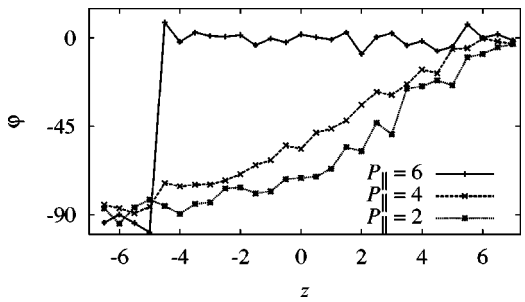

FIG. 12. Twist of azimuthal angle φ of the director $\mathbf{n}(z)$ along the cell for different pressures.

TABLE I. Comparison of phase transition pressures of the isotherm $T=1$ for different kind of geometries.

	Bulk	Homeotropic anchoring	Twisted homogeneous planar anchoring
P_{IN}	1.7	1.5	1.5
P_{NS}	7.4	2.5	4.6
P_{SN}	1.5	1.5	
P_{NI}	1.3	1.2	
P_{SI}			1.2

V. CONCLUDING REMARKS

We observed compression and expansion processes in constant pressure Monte Carlo simulations for a bulk system and in slab geometries with different anchoring mechanisms at the solid walls. For a summary, we compile in Table I pressures at which phase transitions occur at $T=1$. In all three cases the pressure regime for the nematic phase is very narrow in the expansion process or even vanishes (see Figs. 3, 5, and 9). This is because of a large hysteresis, which is typical for first-order phase transitions. The solid state here is very stable. The confinement of flat walls forces the phase transition to be shifted compared with the bulk, especially for solidification and melting. This can be understood because of the positional order, that the wall brings into the system. A first layer beside the wall is formed very early and in this layer it is easy for the system to achieve highly or-

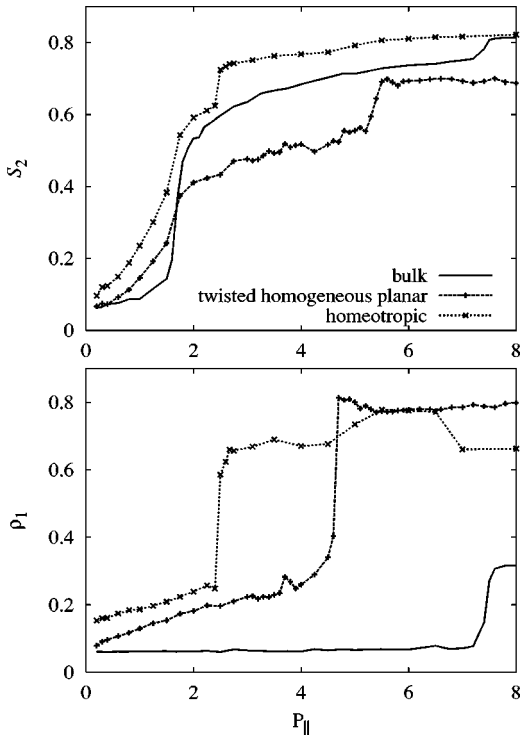

FIG. 13. Comparison of nematic (S_2) and smectic (ϱ_1) order parameters as function of the pressure for the isotherm $T=1$ and different kind of geometries. Only the compression process is shown.

dered states. Figure 13 shows the nematic and smectic order parameter for the compression process each in separate pictures for better comparison. The isotropic-nematic transition is only slightly shifted by the walls towards smaller pressures, the nematic-solid transition is clearly shifted, especially for the homeotropic alignment. In the case of twisted homogeneous planar alignment we found a linear relationship between the azimuthal angle of the director and the z coordinate in the simulation box (Fig. 12). A detailed analysis of the rotating director along the cell including estimates for the twist elastic constant will be presented elsewhere.

The knowledge of the static properties of the bulk fluid and the behavior of the liquid crystal in the vicinity of walls as presented here is a prerequisite for the analysis of dynamic phenomena in confined and in mesoscopically structured systems. It is desirable to study via molecular dynamics simulations the influence of walls on the translational and rotational diffusion and to compare it with results inferred from NMR experiments [45]. Nonequilibrium molecular dynamics simulations of the viscous properties as calculated previously for ellipsoids and Gay-Berne particles [46] should be performed for the model liquid crystal used here. Furthermore, an extension of the present study to fluids of Janus particles [47] is desirable.

ACKNOWLEDGMENTS

This work has been performed under the auspices of the Sonderforschungsbereich 448 ''Mesoskopisch strukturierte Verbundsysteme.'' Financial support by the Deutsche Forschungsgemeinschaft is gratefully acknowledged. We thank Henry Bock (currently at North Carolina State University) and Igor Stanković for help and discussion.

[1] *Liquid Crystals. Applications and Uses*, edited by B. Bahadur (World Scientific, Singapore, 1990), Vol. 1.
[2] A.B. Bračič, K. Kočevar, I. Muševič, and S. Žumer, Phys. Rev. E **68**, 011708 (2003).
[3] M.M. Telo da Gama, Physica A **244**, 389 (1999).
[4] M.K. Chalam, K.E. Gubbins, E. de Miguel, and L.F. Rull, Mol. Phys. **7**, 357 (1991).
[5] Z. Zhang, A. Chakrabarti, O.G. Mouritsen, and M.J. Zuckermann, Phys. Rev. E **53**, 2461 (1996).
[6] G.D. Walls and D.J. Cleaver, Phys. Rev. E **56**, 4306 (1997).
[7] T. Gruhn and M. Schoen, Phys. Rev. E **55**, 2861 (1997).
[8] T. Gruhn and M. Schoen, J. Chem. Phys. **108**, 9124 (1998).
[9] C. Chiccoli, P. Pasini, S. Guzzetti, and C. Zannoni, Mol. Cryst. Liq. Cryst. **360**, 119 (2001).
[10] M. Dijkstra, R. van Roij, and R. Evans, Phys. Rev. E **63**, 051703 (2001).
[11] J. Quintana, E.C. Poiré, H. Domínguez, and J. Alejandre, Mol. Phys. **100**, 2597 (2002).
[12] K. Venu, V.S.S. Sastry, and K.P.N. Murthy, Europhys. Lett. **58**, 646 (2002).
[13] N.V. Priezjev, G. Skačej, R.A. Pelcovits, and S. Zumer, Phys. Rev. E **68**, 041709 (2003).
[14] S. Kondrat, A. Poniewierski, and L. Harnau, Europhys. Lett. **10**, 163 (2003).
[15] R. Memmer and O. Fliegans, Phys. Chem. Chem. Phys. **5**, 558 (2003).
[16] A. Poniewierski and R. Hołyst, Phys. Rev. A **38**, 3721 (1988).
[17] A.M. Somoza, L. Mederos, and D.E. Sullivan, Phys. Rev. E **52**, 5017 (1995).
[18] T.J. Sluckin, Physica A **213**, 105 (1995).
[19] M.M. Telo da Gama, Physica A **172**, 219 (1991).
[20] I. Rodríguez-Ponce, J.M. Romero-Enrique, E. Velasco, L. Mederos, and L. Rull, Phys. Rev. Lett. **82**, 2697 (1999).
[21] A.N. Shalaginov and D.E. Sullivan, Phys. Rev. E **63**, 031704 (2001).
[22] I. Rodríguez-Ponce, J.M. Romero-Enrique, and L. Rull, Phys. Rev. E **64**, 051704 (2001).
[23] M.P. Allen, Mol. Phys. **96**, 1391 (1999).
[24] A. Chrzanowska, P.I.C. Teixeira, H. Ehrentraut, and D.J. Cleaver, J. Phys.: Condens. Matter **13**, 4715 (2001).
[25] D. Andrienko and M.P. Allen, Phys. Rev. E **65**, 021704 (2002).
[26] B.J. Berne and P. Pechukas, J. Chem. Phys. **56**, 4213 (1972).
[27] J.G. Gay and B.J. Berne, J. Chem. Phys. **74**, 3316 (1981).
[28] P.A. Lebwohl and G. Lasher, Phys. Rev. A **6**, 426 (1972).
[29] S. Hess and B. Su, Z. Naturforsch., A: Phys. Sci. **54**, 559 (1999).
[30] H. Steuer, S. Hess, and M. Schoen, Physica A **328**, 322 (2003).
[31] M.P. Allen and D.J. Tildesley, *Computer Simulation of Liquids* (Oxford University Press, Oxford, 1987).
[32] B.K. Peterson and K.E. Gubbins, Mol. Phys. **62**, 215 (1987).
[33] M.P. Allen, J. Chem. Phys. **112**, 5447 (2000).
[34] N. Metropolis, A.W. Rosenbluth, M.N. Rosenbluth, A.H. Teller, and E. Teller, J. Chem. Phys. **21**, 1087 (1953).
[35] I.R. McDonald, Chem. Phys. Lett. **3**, 241 (1969).
[36] M. Schoen, D.J. Diestler, and J.H. Cushman, Phys. Rev. B **47**, 5603 (1993).
[37] M. Schoen, Physica A **270**, 353 (1999).
[38] W. Maier and A. Saupe, Z. Naturforsch. **14a**, 882 (1959).
[39] W. Maier and A. Saupe, Z. Naturforsch. **15a**, 287 (1960).
[40] G. Vertogen and W. H. de Jeu, *Thermotropic Liquid Crystals, Fundamentals*, Springer Series in Chemical Physics (Springer, Berlin, 1988), Vol. 45.
[41] I. Pardowitz and S. Hess, Physica A **100**, 540 (1980).
[42] F. Affouard, M. Kröger, and S. Hess, Phys. Rev. E **54**, 5178 (1996).
[43] M.A. Bates and G.R. Luckhurst, J. Chem. Phys. **110**, 7087 (1999).
[44] T. Riste and L. Dobrzynski, Phys. Rev. Lett. **74**, 2737 (1995).
[45] E. Gedat, A. Schreiber, J. Albrecht, T. Emmler, I. Shenderovich, G.H. Findenegg, H.-H. Limbach, and G. Buntkowsky, J. Phys. Chem. B **106**, 1977 (2002).
[46] S. Hess, in *Advances in the Computer Simulation of Liquid Crystals*, edited by P. Pasini and C. Zannoni (Kluwer, Dordrecht, 2000), pp. 189–233.
[47] T. Erdmann, M. Kröger, and S. Hess, Phys. Rev. E **67**, 041209 (2003).